ORIGINAL PAPER

Biotinylated magnetic nanoparticles for pretargeting: synthesis and characterization study

Ram Prakash Chauhan · Gurjaspreet Singh · Sweta Singh · Narmada Bag · Manoj Patra · S. R. Vadera · Anil K. Mishra · Rashi Mathur

Abstract In this paper, we have proposed a simple method to covalently conjugate biotin to magnetic nanoparticles, which can be targeted to the tumour sites by using pretargeting approach with avidin or streptavidin. Magnetic nanoparticles of manganese ferrite were synthesized by alkaline coprecipitation of ferric chloride hexahydrate, ferrous sulphate heptahydrate and manganese sulphate monohydrate using ammonium hydroxide. The synthesized magnetic nanoparticles were then successfully surface modified by using 3-aminopropyl trimethoxysilane, and the amount of aminopropylsilane bound to the surface of magnetic nanoparticles was quantified by measuring the absorbance of a purple-coloured complex (Ruhemann's purple) formed between amine group and ninhydrin at 576 nm. The aminated magnetic nanoparticles were then conjugated to biotin by reacting them with N-hydroxysuccinimide–biotin in dimethylsulphoxide. The successful conjugation of biotin to magnetic nanoparticles was confirmed by Fourier transform infrared spectroscopy. The size, phase and magnetic nature of the synthesized nanoparticles were analysed by using various techniques like transmission electron microscopy, X-ray diffraction, energy-dispersive X-ray spectroscopy and vibrating sample magnetometry.

R. P. Chauhan · S. Singh · N. Bag · A. K. Mishra · R. Mathur (✉)
Division of Cyclotron and Radiopharmaceutical Sciences,
Institute of Nuclear Medicine and Allied Sciences,
Defence Research and Development Organisation,
Brig.S.K.Mazumdar Marg,
Delhi 110054, India
e-mail: mrrp303@gmail.com

R. Mathur
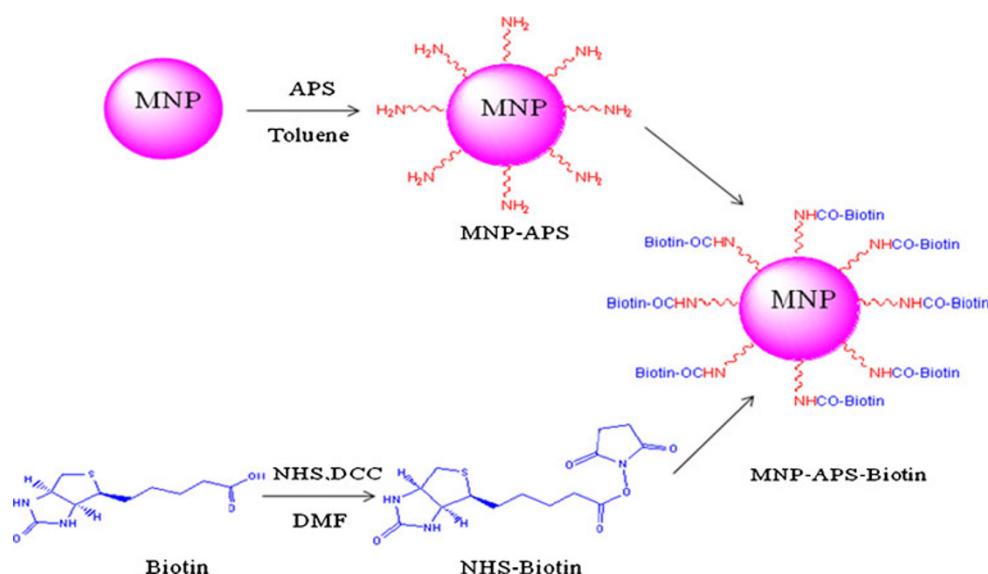e-mail: rashimathur07@gmail.com

R. P. Chauhan · G. Singh
Department of Chemistry, Panjab University,
Chandigarh 160014, India

M. Patra · S. R. Vadera
Defence Laboratory,
Ratanada Palace Road,
Jodhpur 342011, India

1 Introduction

Magnetic particles are interesting candidates for various applications like cell separation (Sieben et al. 2001; Begg et al. 2002), hyperthermia (Hilger et al. 2005), embolotherapy (Lee et al. 2005), targeted drug delivery, diagnosis and therapy (Zhang et al. 2008; Bulte et al. 1992; Go et al. 1993; Kohler et al. 2005) of tumour because of their fine magnetic properties. As magnetic nanoparticles are finding increasing uses day by day, their use for a particular application is mainly governed by their size. Particularly for in vivo applications, their size range plays a very important role, e.g. nanometer-sized particles can be used in diagnosis and therapy of tumours, while particles in the micro range are used in cell separation and embolotherapy. Nowadays, many methods are available to synthesize magnetic nanoparticles, but the need is to develop methods which are easy to apply and can produce magnetic nanoparticles with uniform or narrow size distribution range. Another factor which is important is their stability in vivo, which can be achieved by modifying their surface with some organic molecules that shield them from different physiological conditions within the body post-administration. These molecules provide stealth character to the magnetic nanoparticles by adopting any one of

the three most probable structures as given by Wu et al. (2008), i.e. core shell, mosaic structure and shell core shell structure. In recent years, many approaches have been used for this purpose and also to make them stable. The most common of them is to modify their surface with a biodegradable and biocompatible polymer. Of the various polymers that are commonly employed to make them stable are polyethylene glycol (Zhang et al. 2002), polyvinyl alcohol (Thorek et al. 2006; Cerda et al. 2007), poly-L-lysine (Babic et al. 2008), dextran (Mornet et al. 2005) and carboxymethyl dextran (Horak et al. 2007). All these materials have long chains and functional groups, out of which the chains are adsorbed on the surface of the particles and the functional groups are projected outwards, which helps in providing them stability in physiological medium and also the reacting sites for further modification. Some other molecules which are currently being explored for this purpose are dopamine (Xu et al. 2004), aminopropylsilanes (Iida et al. 2005), amino acids like glutamic acid (Sousa et al. 2001), lysine (Durmus et al. 2009), cystine (White et al. 2009), etc. In this work, we have chosen 3-Aminopropyltrimethoxysilane (APS) (Ma et al. 2003; Yamaura et al. 2004) as surface-modifying agent because of its strong binding ability to various surfaces, as it can form strong covalent bond with them and particularly with the ferrites. The bonding of the ferrites with aminopropyltrialkoxysilanes resulted due to the formation of Fe–O–Si covalent linkage which is quite strong and hence helps further in conjugation because of having free amino group which can be easily modified. The next step in utilizing these nanoparticles for in vivo applications particularly in diagnosis and therapy of tumours is to make them target specific, which can be achieved by modifying their surface with some targeting agents. Various agents that can be used or are currently being explored for targeting tumours are folic acid (Mohapatra et al. 2007; Sudimack and Lee 2000), Arginine–Glycine–Aspartic acid (RGD) peptides (Lee et al. 2009; Su et al. 2002; Montet et al. 2006; Xie et al. 2008; Lee et al. 2008), chlorotoxin (Sun et al. 2008) and various antibody conjugates. Folic acid is quite commonly used to target various types of cancers as its receptors which are glycosylphosphatidylinositol derivatives are overexpressed on many types of cancers including breast, lung, cervical, brain metastasis and renal cell carcinomas (Gabizon et al. 1999; Stella et al. 2000). The RGD peptides which contain arginine–glycine–aspartic acid sequence are used to target $\alpha_v\beta_3$ integrin receptors which are markers of tumour angiogenesis and are significant in early cancer detection. Chlorotoxin, a 36-amino acid peptide, binds specifically to glioma (Veiseh et al. 2005), medulloblastoma, prostate cancer, sarcoma and intestinal cancer (Veiseh et al. 2007) that overexpresses membrane-bound matrix metalloproteinase-2. We chose biotin as an agent to target the magnetic nanoparticles to the tumours because of its strong binding affinity with avidin and streptavidin as the interaction between them is among the strongest known noncovalent interactions which are stable at wide range of temperatures (up to 120°C) and pH (2–13), thus providing a good opportunity for in vivo targeting. Also, the avidin can bind four biotin units per molecule, thus biotin–avidin system provides a very good platform for targeting various biotinylated agents to the tumours. The high isoelectric point (10.5) and good degree of glycosylation (Tannous et al. 2006; Sakahara and Saga 1999) of avidin are other prime actors which help in the tumour uptake of the avidin. Hence,

Fig. 1 A pictorial representation of strategy used for conjugation of biotin to manganese ferrite nanoparticles

APS = 3-Aminopropyltrimethoxysilane, **MNP**= Magnetic nanoparticle
MNP-APS = Aminopropyltrimethoxysilane conjugated magnetic nanoparticle
MNP-APS-Biotin = Biotin conjugated magnetic nanoparticles

the biotin and biotinylated agents can be easily targeted to the tumours by using the affinity of biotin to the avidin. Another plus point of using the biotin–avidin system is that the avidin acts as a chase to remove the extra biotinylated (Tilborg et al. 2008) agent from the circulation and helps in differentiating the targeted site from the background. So, by targeting the magnetic nanoparticles to the tumour sites by exploiting the well-known affinity of biotin and its derivatives to the avidin or streptavidin, great advancements can be achieved in tumour diagnosis using contrast-enhanced magnetic resonance imaging (MRI). The synthetic strategy used for conjugating biotin to magnetic nanoparticles is shown in Fig. 1.

2 Experimental

2.1 Materials

Ferric chloride hexahydrate, ferrous sulphate heptahydrate, manganese sulphate monohydrate, ammonium hydroxide, dimethylsulphoxide (DMSO), N,N-dimethylformamide (DMF), methanol, toluene and diethyl ether were purchased from Merck. Biotin, APS, ninhydrin, N-hydroxysuccinimide (NHS), N,N-dicyclohexylcarbodiimide (DCC) were from Sigma Chemical Co. All chemicals were used as received without further purification until mentioned by the supplier. For all purposes, wherever water is required, ultrapure milli-Q water was used.

2.2 Synthesis of manganese ferrite nanoparticles

Magnetic nanoparticles of manganese ferrite were synthesized by alkaline coprecipitation (Bautista et al. 2005; Lee et al. 2004) of ferric chloride hexahydrate, ferrous sulphate heptahydrate and manganese sulphate monohydrate using ammonium hydroxide. Briefly, 0.086 mol of ferric chloride

Table 1 Measured lattice spacing (d) and standard lattice spacing of manganese ferrite nanoparticles (Lu et al. 2009) with their hkl indexes

Synthesized $MnFe_2O_4$ (Å)	Standard $MnFe_2O_4$ (Å)	hkl indexes
2.95	3.01	220
2.52	2.56	311
2.10	2.12	400
1.72	1.73	422
1.61	1.64	511
1.48	1.50	440
1.27	1.30	533

hexahydrate, 0.0344 mol of ferrous sulphate heptahydrate and 0.0086 mol of manganese sulphate monohydrate were dissolved completely in 50 ml of water, and the resultant metal ion solution was added dropwise to a 50-ml ammonium hydroxide solution under constant stirring followed by sonication. The synthesized suspension of magnetic nanoparticles was then collected on a Whatman filter paper, washed with water till the filtrate is free of alkalinity and dried in an oven (60–70°C) to obtain brown powder of magnetic nanoparticles.

2.3 Surface modification of magnetic nanoparticles with 3-Aminopropyltrimethoxysilane

The conjugation of APS (Xu et al. 1997) to the surface of the magnetic nanoparticles was done by dispersing 50 mg of magnetic nanoparticles in 25 ml of toluene under sonication for 20 min and then adding 250 mg of 3-aminopropyl trimethoxysilane to it and kept stirring the reaction mixture for 24 h at room temperature. The aminated magnetic nanoparticles were then collected by using a magnet and were then washed two times with toluene and three times with methanol and were then
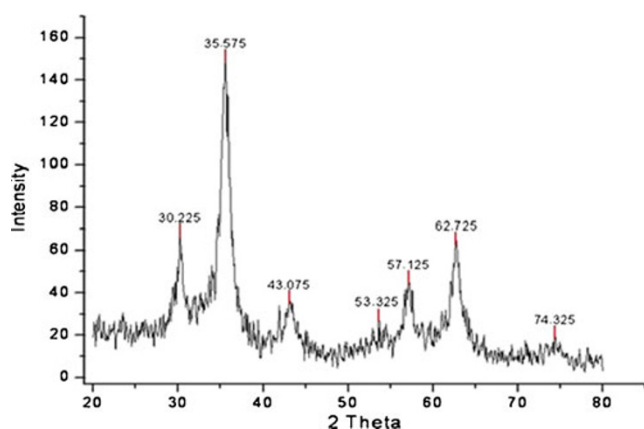

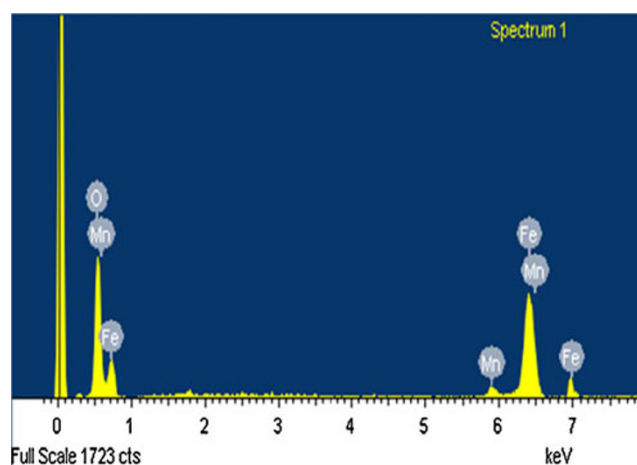**Fig. 2** X-ray diffraction spectrum of synthesized manganese ferrite nanoparticles

Fig. 3 EDX spectrum of synthesized manganese ferrite nanoparticles

dried in an oven at 50°C and were stored in a vacuum desiccator.
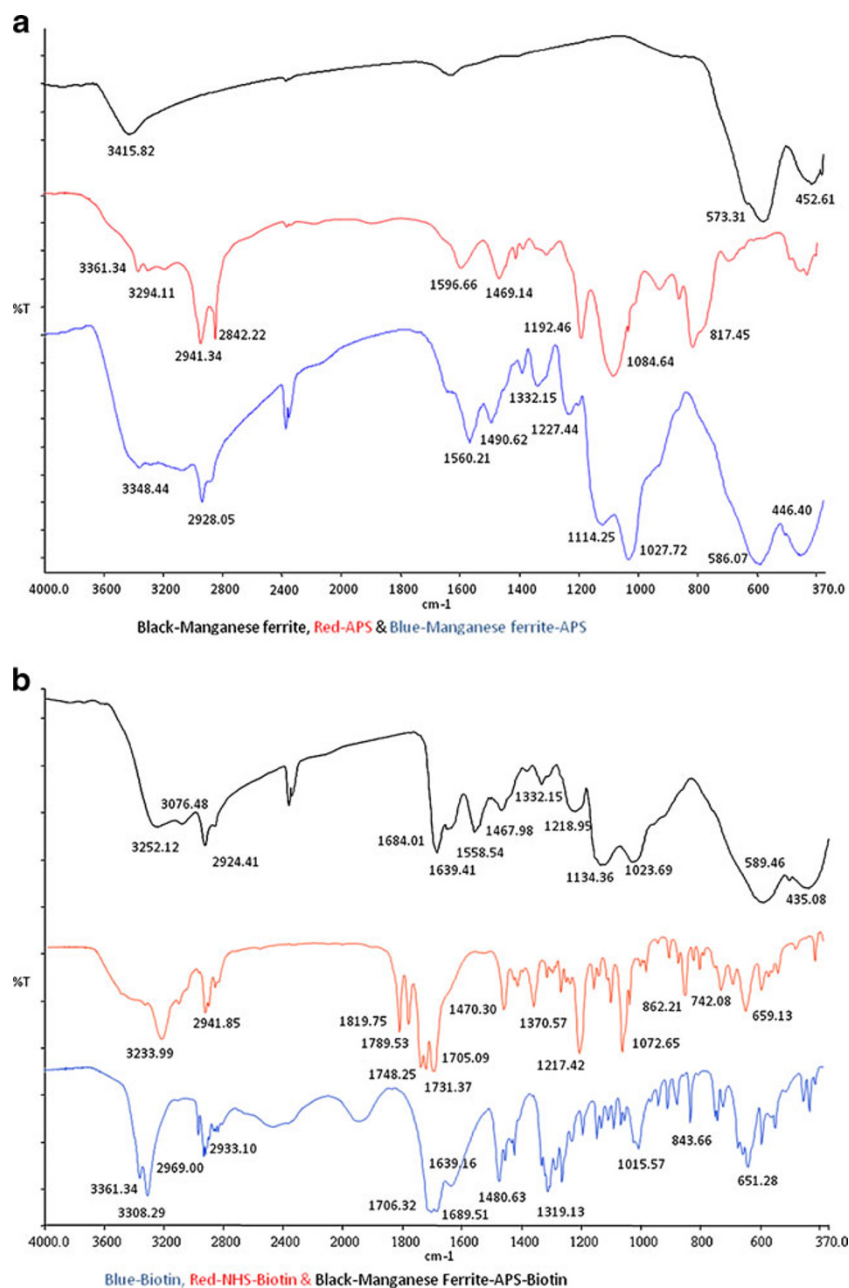
2.4 Synthesis of N-hydroxysuccinimide–biotin

N-Hydroxysuccinimide–biotin (NHS–biotin) was synthesized according to earlier reported procedure (Susumu et al. 2007) by reacting biotin with N-hydroxysuccinimide (NHS) and DCC in a molar ratio of 1:1.1:1.2 in dry DMF under nitrogen atmosphere at 35°C for 24 h. The crude NHS–biotin was stored at 4°C to crystallize out dicyclohexylurea crystals which were then removed by filtering. The NHS–biotin was then precipitated by adding ten times

volume of cold diethyl ether and was again washed with ether.

2.5 Conjugation of NHS–biotin to aminated magnetic nanoparticles

For conjugating biotin to aminopropyl trimethoxysilane-modified magnetic nanoparticles, 108 mg of NHS–biotin was dissolved in 5 ml of dry DMSO, and then, 12 mg of 3-aminopropyl trimethoxysilane-modified magnetic nanoparticles were added to it and kept stirring the reaction mixture for 48 h. The resulting biotinylated magnetic nanoparticle suspension was then centrifuged

Fig. 4 **a** FTIR spectra of as synthesized manganese ferrite nanoparticles (*black*), APS (*red*) and APS conjugated manganese ferrite nanoparticles (*blue*). **b** FTIR spectra of biotin (*blue*), NHS-biotin (*red*), biotin conjugated manganese ferrite nanoparticles (*black*)

at 10,000 rpm at 4–5°C for 10 min so as to collect the biotinylated magnetic nanoparticles which were then washed eight to nine times with ultrapure milli-Q water so as to completely remove DMSO. The resulting biotinylated magnetic nanoparticles were then dried in an oven at 50°C and stored in a vacuum desiccator.

2.6 Characterization

Phase identification of the synthesized metal ferrite nanoparticles was done by powder X-ray diffraction method using CuKα_1 (1.54060 A^0) radiation on X-Pert Pro-Pan analytical model, and the average particle size was calculated using Scherer equation (i.e. $t=0.9\lambda$/B cos θ). Fourier transform infrared spectroscopy (FTIR) spectra of all samples in the range of 400–4,000 cm^{-1} were recorded by using KBr pellet method using Perkin Elmer, Spectrum-BXII FTIR Instrument. UV–visible measurements were carried out by using double beam UV–Visible spectrophotometer 5704SS model, Electronics Corporation of India Limited. Morphology and particle sizes were examined by using a transmission electron microscope (TEM). Magnetic measurement study was carried out by using Vibrating Sample Magnetometer (VSM) ADE model EG5. Nuclear magnetic resonance (NMR) spectra

Table 2 Assignment of FTIR spectra of as-synthesized manganese ferrite nanoparticles, APS, APS-modified manganese ferrite, biotin, NHS–biotin and biotin-conjugated manganese ferrite nanoparticles

Samples	Stretching frequency (cm^{-1})	Vibrational mode
	3,415	ν (O–H)
Manganese ferrite	573,452	M–O stretching
3-Aminopropyltrimethoxysilane (APS)	3,361, 3,294	ν_{as} (N–H) and ν_s (N–H)
	2,941, 2,842	ν_{as} (C–H) and ν_s (C–H)
	1,596	δ (NH$_2$)
	1,469	δ (C–H)
	1,192, 1,084	Si–O–C stretching
	3,348	ν (N–H)
APS-modified manganese ferrite	2,928	ν (C–H)
	1,560	δ (NH$_2$)
	1,490	δ (C–H)
	1,114, 1,027	Si–O–Si and Si–O–Fe linkages
	586,446	M–O stretching
	3,361	ν (O–H) of –COOH
	3,308	ν (N–H)
Biotin	2,969, 2,933	ν_{as} (C–H) and ν_s (C–H)
	1,706, 1,689	ν (C=O) of –COOH
	1,639	ν (C=O) of –CONH
	1,480, 1,319	δ (C–H) and δ (NH)
	1,015	ν (C–O) of –COOH
	3,233	ν (N–H)
	2,941	ν (C–H)
NHS–biotin	1,819, 1,789	ν (C=O)
	1,748, 1,731, 1,705	ν (C=O)
	1,470, 1,370	δ (C–H) and δ (NH)
	1,217, 1,072	ν (N–O) and ν (C–O) of ester
	3,252	ν (N–H)
	2,924	ν (C–H)
Biotin-conjugated manganese ferrite	1,684	ν (C=O) amide I
	1,558	δ (N–H) amide II
	1,467	δ (C–H)
	1,134, 1,023	Si–O–Si and Si–O–Fe linkages
	589,435	M–O stretching

were taken on a Bruker 400 MHz NMR spectrometer. Mass spectrum was recorded using Agilent 6310 ion trap LCMS.

3 Results and discussion

3.1 X-ray diffraction study

X-ray diffraction spectrum of synthesized magnetic nanoparticles (Fig. 2) shows peaks at $2\theta=30°$ (220), 35° (311), 43° (400), 53° (422), 57° (511), 63° (440) and 74° (533) which corresponds to the spinel phase. Lattice spacing measurements are in close agreement with those with the standard spacing of manganese ferrite (Lu et al. 2009) at their respective hkl indexes (Table 1), which proves that the synthesized nanoparticles are of manganese ferrite. Further, the occurrence of broadness at the base of peaks indicates that the particle size is very small. Average crystallite size calculated using Debye–Scherer equation (i.e. $t=0.9\lambda/B\cos\theta$) is around 10.46 nm.

3.2 Energy-dispersive X-ray spectroscopy study

The energy-dispersive X-ray spectroscopy (EDX) spectrum of synthesized manganese ferrite nanoparticles (Fig. 3) shows peaks corresponding to energy of X-ray emitted, which is characteristic of manganese and iron. This again supports our X-ray diffraction (XRD) results that the synthesized nanoparticles are of manganese ferrite. The weight percentage of manganese calculated using EDX analysis is found to be 4.09% which is very close to the experimental used percentage of manganese which is 4.24%, and the weight ratio of Mn/Fe/O is found to be 4.09:58.69:37.22.

3.3 FTIR spectroscopic study

The successful conjugation of APS to the surface of magnetic nanoparticles is proved by FTIR. The major peaks in the spectra (Fig. 4a) of manganese ferrite were assigned to M–O str. at 573 and 452 cm^{-1}. The peaks in the spectra of APS were due to N–H str. (asym and sym) at 3,361 and 3,294 cm^{-1}, C–H str. (asym and sym) at 2,941 and 2,842 cm^{-1}, N–H $_{def}$ at 1,596 cm^{-1}, C–H $_{def}$ at 1,469 cm^{-1}, 1,192 and 1,084 cm^{-1} due to Si–O–C stretching. The peaks in the spectra of APS-conjugated manganese ferrite were 3,348 cm^{-1} (N–H str.), 2,928 cm^{-1} (C–H str.), 1,560 (N–H $_{def}$), 1,490 (C–H $_{def}$), 1,114 and 1,027 cm^{-1} due to Si–O–Si and Fe–O–Si linkages, 586 and 446 cm^{-1} due to M–O str. By comparison of the infrared (IR) spectra of synthesized manganese ferrite nanoparticles, APS and APS-modified magnetic nanoparticles, we can clearly see a major shift in the various modes of vibrations
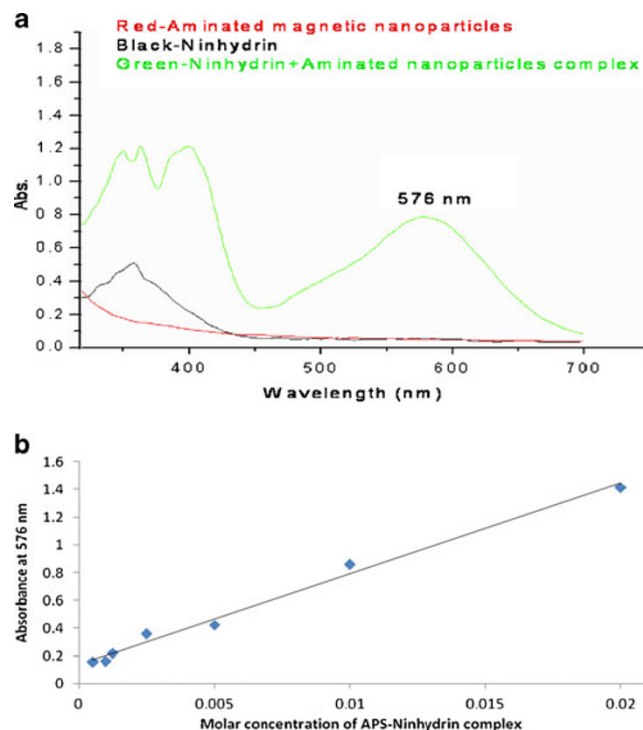

Fig. 5 a UV–visible absorbance spectra of aminated magnetic nanoparticles (*red*), ninhydrin (*black*) and ninhydrin complex of aminated nanoparticles (*green*). **b** Plot of molar concentration of APS–ninhydrin complex versus absorbance at 576 nm
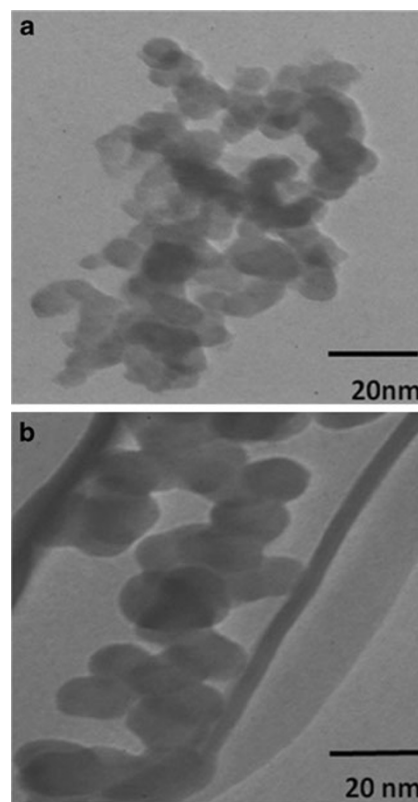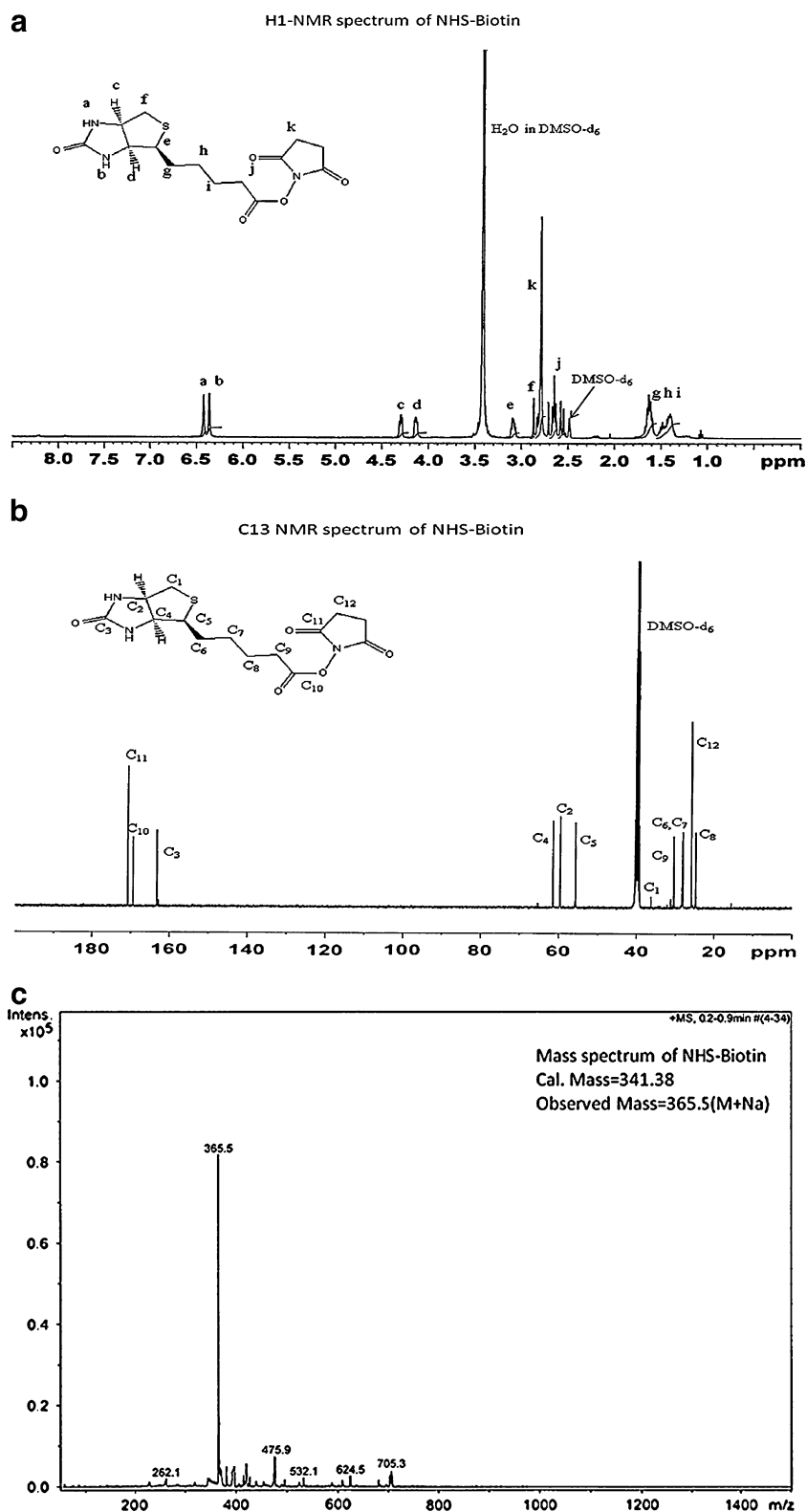

Fig. 6 a TEM image of synthesized manganese ferrite nanoparticles. **b** TEM image of biotin-conjugated manganese ferrite nanoparticles

which proves that APS is successfully conjugated covalently to the surface of magnetic nanoparticles. The successful conjugation of biotin to the aminated nanoparticles is explained clearly by comparing the IR spectra of biotin, NHS–biotin and biotinylated magnetic nanoparticles (Fig. 4b). The peaks in the spectra of biotin-conjugated magnetic nanoparticles were 3,252 cm^{-1} (N–H str.), 3,076, 2,924 cm^{-1}(C–H str.), 1,684 cm^{-1} (C=O str.), 1,640 cm^{-1}

Fig. 7 **a** ^{1}H-NMR spectrum of NHS–biotin. **b** ^{13}C-NMR spectrum of NHS–biotin. **c** Mass spectrum of NHS–biotin

(C=O str.), 1,558 cm^{-1} (N–H $_{def}$), 1,467 cm^{-1} (C–H $_{def}$), 1,134 and 1,023 cm^{-1} (Si–O–Si and Si–O–Fe) linkages, 589 and 435 cm^{-1} due to M–O str. A comparison of the different vibrational modes of manganese ferrite nanoparticles, APS, APS-modified manganese ferrite, biotin, NHS–biotin and biotinylated magnetic nanoparticles is given in Table 2.

3.4 UV–visible spectroscopy study

The presence of APS bound to the surface of nanoparticles was also confirmed by UV–visible spectroscopy in addition to FTIR and estimated quantitatively by measuring the absorbance of the purple-coloured complex formed by its reaction with ninhydrin. Ninhydrin, on reaction with amino group containing compounds like amines and amino acids, forms a purple-coloured (McCaldin 1960; Rahman and Kashif 2003) complex (Ruhemann's purple) which absorbs at 576 nm. For determining quantitatively the amount of APS bound to the surface of the nanoparticles, a plot of molar concentration versus absorbance (at 576 nm) of ninhydrin complex of pure APS was drawn, and then, the amount of APS bound to the surface of nanoparticles was determined from the graph. The UV–visible absorbance spectrum of ninhydrin complex of aminated magnetic nanoparticles is shown in Fig. 5a. The presence of a band at 576 nm due to the formation of a purple-coloured complex between APS conjugated to magnetic nanoparticles and ninhydrin again proves the presence of APS on the surface of magnetic nanoparticles. For UV–visible measurements, all samples were prepared in methanol. The amount of APS bound to the surface of nanoparticles, determined by plotting the absorbances obtained at 576 nm versus different concentrations of APS–ninhydrin complex

(Fig. 5b), was found to be 2.68×10^{-5} mol per milligram of magnetic nanoparticles which is slightly lesser than the theoretical value of 2.79×10^{-5} mol.

3.5 Transmission electron microscopy

The TEM image of bare manganese ferrite nanoparticles (Fig. 6a) shows that particles are nearly spherical in shape with slight aggregation and having size in the range of (10±4) nm which is very close to that measured by XRD. The TEM image of biotin-conjugated manganese ferrite nanoparticles (Fig. 6b) also shows spherical particles with almost the same size, but their aggregation is reduced as compared to bare particles.
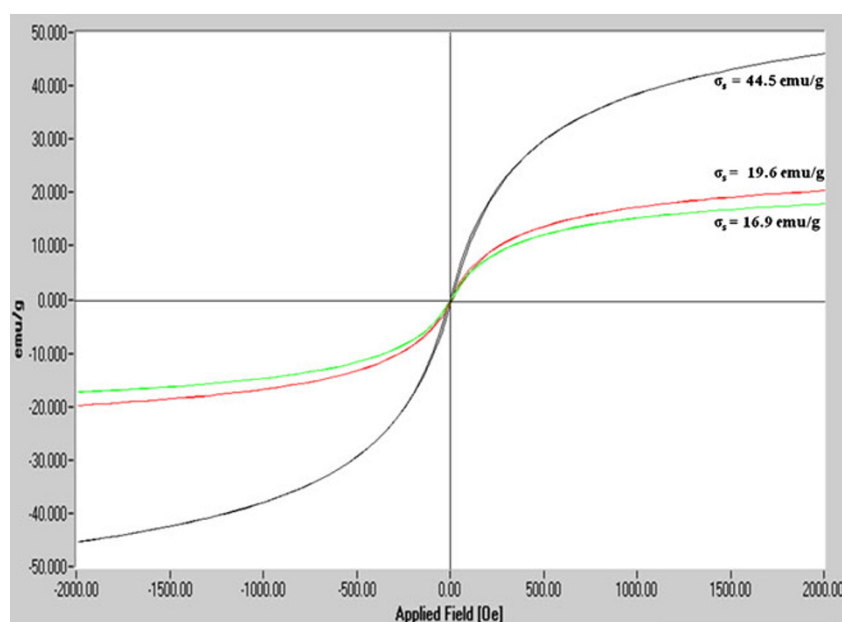
3.6 NMR spectroscopic and mass spectrometric study

The synthesis of NHS–biotin was confirmed by proton NMR (^{1}H-NMR; Fig. 7a), carbon NMR (^{13}C-NMR; Fig. 7b) and mass (Fig. 7c) spectrometry. The following are the details: ^{1}H-NMR (400 MHz, DMSO-d$_6$), δ 6.42 (s, 1H, N–H), 6.36 (s, 1H, N–H), 4.29 (t, 1H), 4.13 (t, 1H), 3.09 (m, 1H), 2.79 (s, 4H), 2.65 (t, 2H), 1.63 (m, 2H), 1.43 (m, 2H), 1.39 (m, 2H). ^{13}C-NMR 170.7, 169.4, 163.2, 61.4, 59.6, 55.8, 36.3, 31.2, 28.5, 28.2 25.8, 24.8 Mass spectrum (electron spray ionization); ion polarity, positive; calculated mass=341.38 ($C_{14}H_{19}N_3O_5S$); observed mass=365.5 due to [M+Na]$^+$.

3.7 Vibrating sample magnetometer study

By comparison of the magnetic susceptibility measurement graphs (Fig. 8) of synthesized manganese ferrite

Fig. 8 Magnetization curve of synthesized manganese ferrite (black), APS conjugated manganese ferrite (red) and biotin conjugated manganese ferrite (green) nanoparticles clearly showing super paramagnetic behaviour

σ_s = 44.5 emu/g
σ_s = 19.6 emu/g
σ_s = 16.9 emu/g

nanoparticles (σ_s=44.5 emu/g), APS-modified nanoparticles (σ_s=19.6 emu/g) and that of biotinylated manganese ferrite nanoparticles (σ_s=16.9 emu/g), we can clearly see a decrease in saturation magnetization after conjugation of APS and biotin. This decrease in saturation magnetization is due to the diamagnetic contribution from these surface-conjugated (APS and biotin) organic molecules which reduces the net magnetization. To elaborate further, the reason behind the reduction in saturation magnetization is that the overall size of the particle increases after conjugation of these organic molecules, but the size of the core remains the same as the reaction takes place only on the surface of the particle. So, after conjugation of these organic molecules, the overall particle size goes on increasing due to increase in the thickness of the organic layer around the core as we found later, but the core size remains the same, and as we know that the magnetism is only due to the core, so there is a decrease in saturation magnetization after conjugation of APS and biotin. By using the formula [$\sigma_s = \sigma_{s\ (bulk)}\ (1-6t/d)$] for calculating the thickness (t) of dead layer on the surface of magnetic nanoparticles and using the saturation magnetization value of bulk manganese ferrite (80 emu/g) as given by Zheng et al. (1998) and also by putting the average size (d), i.e. 10.4 nm in our case, the thickness of APS and biotin was found to be 0.53 and 0.07 nm, respectively. The thickness of APS and biotin layer obtained from magnetization data shows that after conjugation of APS, the increase in size was 0.53 nm and decrease in magnetization was 24.9 magnetization units, and after conjugation of biotin, size increase was 0.07 nm only w.r.t. APS-conjugated magnetic nanoparticles. This biotin layer formed is very thin as compared to the APS layer; therefore, there was a small decrease (2.7 units) in magnetization after conjugation of biotin. The total increase in thickness after conjugation of both APS and biotin is so small (i.e. only 0.60 nm) that it is not detectable in normal TEM instruments as observed from our TEM results. From Fig. 8, it is clear that all three samples are typically super paramagnetic in nature with no noticeable hysteresis. But to our interest, magnetic nanoparticles retained their super paramagnetic behaviour even after surface conjugation of biotin, which is good for exploiting it in contrast-enhanced MRI by using the ability of biotin and biotinylated agents to bind to avidin-pretargeted sites.

4 Conclusion

We developed a method to conjugate biotin to the surface of magnetic nanoparticles by using a simple and easy to apply chemical approach. The amount of APS bound to magnetic nanoparticles was determined quantitatively by using ninhydrin. Employing the formula reported earlier for determining the thickness of dead layer on the surface of magnetic nanoparticles, we successfully calculated the thickness of APS and biotin layer bound to the surface of magnetic nanoparticles. The successful conjugation of biotin to magnetic nanoparticles and their super paramagnetic behaviour, evident from FTIR and VSM, suggest that the synthesized biotinylated magnetic nanoparticles could be a useful agent in contrast-enhanced MRI.

References

Babic M, Horak D, Trchova M, Jendelova P, Glogarova K, Sykova E et al (2008) Poly(L-lysine)-modified iron oxide nanoparticles for stem cell labeling. Bioconj Chem 19:740–750

Bautista MC, Miguel OB, Morales MP, Serna CJ, Verdaguer SV (2005) Surface characterisation of dextran-coated iron oxide nanoparticles prepared by laser pyrolysis and coprecipitation. J Magn Magn Mat 293:20–27

Begg AC, Sprong D, Balm A, Martin JMC (2002) Premature chromosome condensation and cell separation studies in biopsies from head and neck tumors for radiosensitivity prediction. Radiother Oncol 62:335–343

Bulte JW, Hoekstra Y, Kamman RL, Magin RL, Webb AG, Miltenyi S et al (1992) Specific MR imaging of human lymphocytes by monoclonal antibody-guided dextran-magnetite particles. Magn Reson Med 25:148–157

Cerda LAG, Castro MUE, Zertuche MS (2007) Preparation and characterization of polyvinyl alcohol–cobalt ferrite nanocomposites. J Non Cryst Sol 353:808–810

Durmus Z, Toprak MS, Baykal A, Altmcekic TG, Bozkurt A, Cosgun S et al (2009) L-lysine coated iron oxide nanoparticles: synthesis, structural and conductivity characterization. J Alloys Compd 484:371–376

Gabizon A, Horowitz AT, Goren D, Tzemach D, Mandelbaum SF, Zalipsky S (1999) Targeting folate receptor with folate linked to extremities of poly(ethylene glycol)-grafted liposomes: in vitro studies. Bioconj Chem 10:289–298

Go KG, Bulte JW, de Ley L, Hulstaert CE, Blaauw EH, Ma LD et al (1993) Our approach towards developing a specific tumour-targeted MRI contrast agent for the brain. Eur J Radiol 16:171–175

Hilger I, Hergt R, Kaiser WA (2005) Towards breast cancer treatment by magnetic heating. J Magn Magn Mat 293:314–319

Horak D, Petrovsky E, Kapick A, Frederichs T (2007) Synthesis and characterization of magnetic poly(glycidyl methacrylate) microspheres. J Magn Magn Mat 311:500–506

Iida H, Nakanishi T, Osaka T (2005) Surface modification of γ-Fe2O3 nanoparticles with aminopropylsilyl groups and interparticle linkage with α, ω-dicarboxylic acids. Electrochim Acta 51:855–859

Kohler N, Sun C, Wang J, Zhang M (2005) Methotrexate modified superparamagnetic nanoparticles and their intracellular uptake into human cancer cells. Langmuir 21:8858–8864

Lee SJ, Jeong JR, Shin SC, Kim JC, Kim JD (2004) Synthesis and characterization of superparamagnetic maghemite nanoparticles prepared by coprecipitation technique. J Magn Magn Mat 282:147–150

Lee HS, Kim EH, Shao H, Kwak BK (2005) Synthesis of SPIO-chitosan microspheres for MRI-detectable embolotherapy. J Magn Magn Mat 293:102–105

Lee HY, Chen K, Hsu AR, Xie J, Sun S, Chen X et al (2008) PET/MRI dual-modality tumor imaging using arginine-glycine-aspartic (RGD)-conjugated radiolabeled iron oxide nanoparticles. J Nucl Med 49:1371–1379

Lee JH, Lee K, Moon SH, Lee Y, Park TG, Cheon J (2009) All-in-one target-cell-specific magnetic nanoparticles for simultaneous molecular imaging and siRNA delivery. Angew Chem Int Ed 48:4174–4179

Lu J, Sun J, Wang Z, Zhao X, Shuai X, Gu Z et al (2009) Manganese ferrite nanoparticle micellar nanocomposites as MRI contrast agent for liver imaging. Biomaterials 30:2919–2928

Ma M, Zhang Y, Yu W, Shen H, Zhang H, Gu N (2003) Preparation and characterization of magnetite nanoparticles coated by amino silane. Coll Surf A Physicochem Eng Asp 212:219–226

McCaldin DJ (1960) The chemistry of ninhydrin. Chem Rev 60:39–51

Mohapatra S, Mallick SK, Maiti TK, Ghosh SK, Pramanik P (2007) Synthesis of highly stable folic acid conjugated magnetite nanoparticles for targeting cancer cells. Nanotechnology 18 (385102):1–9

Montet X, Funovics M, Abou KM, Weissleder R, Josephson L (2006) Multivalent effects of RGD peptides obtained by nanoparticle display. J Med Chem 49:6087–6093

Mornet S, Portier J, Duguet E (2005) A method for synthesis and functionalization of ultrasmall superparamagnetic covalent carriers based on maghemite and dextran. J Magn Magn Mat 293:127–134

Rahman N, Kashif M (2003) Application of ninhydrin to spectrophotometric determination of famotidine in drug formulations. IL Farmaco 58:1045–1050

Sakahara H, Saga T (1999) Avidin–biotin system for delivery of diagnostic agents. Adv Drug Del Rev 37:89–101

Sieben S, Bergemann C, Lube A, Brockmann B, Rescheleit D (2001) Comparison of different particles and methods for magnetic isolation of circulating tumor cells. J Magn Magn Mat 225:175–179

Sousa MH, Rubim JC, Sobrinho PG, Tourinho FA (2001) Biocompatible magnetic fluid precursors based on aspartic and glutamic acid modified maghemite nanostructures. J Magn Magn Mat 225:67–72

Stella B, Arpico S, Peracchia MT, Hoebeke J, Angelo DJ, Couvreur P et al (2000) Design of folic acid-conjugated nanoparticles for drug targeting. J Pharma Sci 89:1452–1464

Su ZF, Liu G, Gupta S, Zhu Z, Rusckowski M, Hnatowich DJ (2002) In vitro and in vivo evaluation of a Technetium-99m-labeled Cyclic RGD peptide as a specific marker of $\alpha_v\beta_3$ integrin for tumor imaging. Bioconj Chem 13:561–570

Sudimack J, Lee RJ (2000) Targeted drug delivery via the folate receptor. Adv Drug Deliv Rev 41:147–162

Sun C, Fang C, Hansen S, Ellenbogen RG, Olson J, Zhang M et al (2008) In vivo MRI detection of gliomas by chlorotoxin-conjugated superparamagnetic nanoprobes. Small 4:372–379

Susumu K, Uyeda HT, Medintz IL, Pons T, Delehanty JB, Mattoussi H (2007) Enhancing the stability and biological functionalities of quantum dots via compact multifunctional ligands. J Am Chem Soc 129:13987–13996

Tannous BA, Grimm J, Perry KF, Chen JW, Weissleder R, Breakefield XO (2006) Metabolic biotinylation of cell surface receptors for in vivo imaging. Nature Methods 3:391–396

Thorek DLJ, Chen AK, Czupryna J, Tsourkas A (2006) Super-paramagnetic iron oxide nanoparticle probes for molecular imaging. Ann Biomed Eng 34:23–38

Tilborg GFV, Strijkers GJ, Pouget EM, Sommerdijk NJM, Nicolay K, Mulder WJM et al (2008) Kinetics of avidin-induced clearance of biotinylated bimodal liposomes for improved MR molecular imaging. Magn Reson Medi 60:1444–1456

Veiseh O, Kohler N, Lee D, Ellenbogen R, Olson J, Zhang M et al (2005) Optical and MRI multifunctional nanoprobe for targeting gliomas. Nano Lett 5:1003–1008

Veiseh M, Zhang M, Hansen SJ, Greenberg NM, Ellenbogen RG, Olson JM et al (2007) Tumor paint: a chlorotoxin:Cy5.5 bioconjugate for intraoperative visualization of cancer foci. Cancer Res 67:6882–6888

White BR, Stackhouse BT, Holcombe JA (2009) Magnetic γ-Fe2O3 nanoparticles coated with poly-L-cysteine for chelation of As (III), Cu(II), Cd(II), Ni(II), Pb(II) and Zn(II). J Hazard Mat 161:848–853

Wu W, He Q, Jiang C (2008) Magnetic iron oxide nanoparticles: synthesis and surface functionalization strategies. Nanoscale Res Lett 3:397–415

Xie J, Chen K, Lee HY, Peng S, Chen X, Sun S et al (2008) Ultrasmall c (RGDyK)-coated Fe3O4 nanoparticles and their specific targeting to integrin $\alpha_v\beta_3$-rich tumor cells. J Am Chem Soc 130:7542–7543

Xu Z, Liu Q, Finch JA (1997) Silanation and stability of 3-aminopropyl triethoxy silane on nanosized superparamagnetic particles: I. Direct silanation. Appl Surf Sci 120:269–278

Xu C, Zheng R, Liu H, Zhang X, Guo Z, Xu B (2004) Dopamine as a robust anchor to immobilize functional molecules on the iron oxide shell of magnetic nanoparticles. J Am Chem Soc 126:9938–9939

Yamaura M, Camilo RL, Sampaio LC, Macedo MA, Nakamura M, Toma HE (2004) Preparation and characterization of (3-aminopropyl) triethoxysilane-coated magnetite nanoparticles. J Magn Magn Mat 279:210–217

Zhang Y, Kohler N, Zhang M (2002) Surface modification of superparamagnetic magnetite nanoparticles and their intracellular uptake. Biomaterials 23:1553–1561

Zhang J, Rana S, Srivastava RS, Misra RDK (2008) On the chemical synthesis and drug delivery response of folate receptor-activated, polyethylene glycol-functionalized magnetite nanoparticles. Acta Biomater 4:40–48

Zheng M, Wu XC, Zou BS, Wang YJ (1998) Magnetic properties of nanosized MnFe2O4 particles. J Magn Magn Mat 183:152–156